A DC-DC Converter with Extended Voltage Static Gain, Input/Output Continuous Current and Reduced Switch Voltage Stress

Joaquim Monteiro
UnIRE, ISEL, Polytechnic University of Lisbon, Portugal
INESC-ID Lisboa, Portugal
0000-0003-1930-9123

V. Fernão Pires
ESTSetúbal, Instituto Politécnico Setúbal, Setubal Portugal
INESC-ID Lisboa, Portugal
0000-0002-3764-0955

Daniel Foito
ESTSetúbal, Instituto Politécnico Setúbal, Setubal Portugal
CTS-UNINOVA, Portugal
0000-0003-4831-9064

J. Fernando Silva
DEEC, IST, Universidade de Lisboa, Lisboa, Portugal
INESC-ID Lisboa, Portugal
0000-0003-2164-0739

Sónia Pinto
DEEC, IST, Universidade de Lisboa, Lisboa, Portugal
INESC-ID Lisboa, Portugal
0000-0003-3266-7881

2024 XV International Symposium on Industrial Electronics and Applications (INDEL) | 979-8-3503-5232-0/24/$31.00 ©2024 IEEE | DOI: 10.1109/INDEL62640.2024.10772678

Abstract— **In recent decades, DC-DC converters have been important to help the penetration of renewable energy sources into the power grid and for use as independent power sources. These power converters are commonly used in many power conversion appliances and portable electronic devices. However, to regulate and convert a photovoltaic (PV) power source voltage to the required output voltage, it is often necessary to use DC-DC converters to provide a stable and adjustable voltage, a feature that most of these converters do not guarantee. Thus, this paper presents a new single-switch DC-DC converter with Boost characteristics. This converter is characterized by extended static voltage gains and input/output currents. Besides, differently to the standard Boost, the voltage stress of the proposed converter switch is lower than the converter output voltage. The proposed converter operating principle and static gain will be examined through theoretical analysis. Some simulation and experimental tests will evaluate its performance and other particularities of this DC-DC converter.**

Keywords - DC/DC Converter, Single-switch; Boost converter, Extended Voltage Static Gain

I. INTRODUCTION

Renewable energy sources are playing an increasingly important role in the energy sector. Among the numerous renewable energy sources available today, solar photovoltaic (PV) has been playing a crucial role. This trend can be largely attributed to several factors of the PV systems, including the minimal environmental impact of energy generation, an immense natural energy source, the ability to be installed in several sunny places, and the ease of installation, operation, and maintenance. However, to interconnect the DC low voltage of solar panels to the power grid, high gain step-up DC-DC intermediate converters are required [1-3]. This kind of power converters is also required in consumer electronics, lighting devices, electric vehicles, and their chargers, as well as in many other industrial applications [4-8]. In addition to these applications, they are widely used in energy generation from renewable sources, particularly for the integration of renewable energy sources into the electrical power grid. [9-11]. One important feature of these DC-DC converters is their ability to regulate the voltage supplied by the PV power source, providing a stable and adjustable output voltage required by AC inverters [12]. Additionally, DC-DC converters present many other features, such as reliability, high efficiency, low maintenance, reduced size, and low cost, making them attractive for many industrial applications [13].

Many DC-DC converters based on standard topologies have been developed and proposed in the literature to enhance certain features. However, for renewable energy applications requiring high voltage gain, many of these solutions only achieve the needed gain using duty cycle extreme values. This operating point, however, leads to increased losses and costs, degrades system performance, and results in low efficiency [14]. For PV systems a DC-DC converter must provide a high step-up voltage gain and high efficiency to raise the low voltage generated by PV panels to a suitable level for further use [15-19]. In this regard, to boost the output voltage, a step-up topology, such as the standard DC-DC boost converter with continuous input current, can be used [20-22]. However, in most topologies the voltage gain is significantly limited due to the parasitic elements of inductors, capacitors, and switching semiconductors [23]. In fact, many research efforts have been done get a high voltage gain. In many research works, using different techniques extended voltage gains led to quadratic voltage gains [24-26]. Unfortunately, most of these configurations need high component count, presenting challenges in terms of control due to their complexity.

Under the previous context, a new contribution regarding a novel topology of the single-switch DC-DC converter with Boost characteristics is proposed. This structure stands out due to its enhanced static voltage gain and input/output continuous current, which improves the overall performance. Indeed, this new converter structure is ideal for several applications requiring extended voltage static gain, such as fuel cells and solar PV panels under shading. Furthermore, the proposed converter ensures stable operation under different conditions by efficiently managing both input and output currents. The design aims to optimize energy conversion and increase the efficiency of power systems. In addition, this converter operates with reduced voltage stress on the power semiconductor and reduced ripple in the input current. The performance of the proposed DC-DC converter topology will be shown through the presentation of several simulations and experiments obtained using computer platforms and a laboratory prototype, respectively.

979-8-3503-5232-0/24/$31.00 ©2024 IEEE

II. DC-DC Converter Topology and Dynamics

Photovoltaic panels connected in series under shading conditions may require individual DC-DC converters that can handle a wide range of input voltages and provide a wide range of output voltages, both above and below the input voltage, to adapt to the most demanding shading conditions. In this regard, this paper suggests the development of a novel DC-DC converter that employs a single-power semiconductor and a straightforward control circuit. The structure of the proposed DC-DC converter is illustrated in Fig. 1. Operating in the continuous conduction mode (CCM) this converter presents low ripple input current, reduced voltage switch stress, and wide range of voltage conversion.

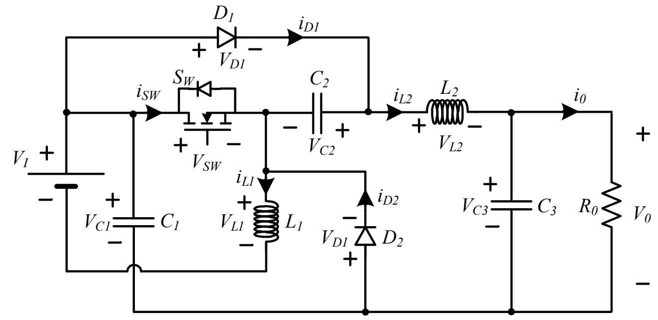

Fig. 1. The DC-DC converter topology proposed

To simplify the study of this converter operating modes, ideal switches, inductors and capacitors are assumed together with operation at steady-state in CCM. Considering T_S the switching period and δ the duty-cycle, the following operation modes can be described:

Switch S_W in ON state: Based on the equivalent circuit presented in Fig. 2, during the ON state the transistor S_W is *ON* during the time interval from *0* to δT_S. In the *ON*-state, diodes D_1 and D_2 are reverse-biased, while currents in both inductors (L_1 and L_2) increases, as the input power source V_I transfers energy to them. On the other hand, the capacitors C_1 and C_2 are in discharging mode and capacitor C_3 in charging mode. In this case the voltage applied to the load is the voltage across C_3. The state variable dynamics are given by (1).

$$\frac{di_{L1}}{dt}=\frac{V_I}{L_1};\quad \frac{di_{L2}}{dt}=\frac{V_I+V_{C2}-V_{C3}}{L_2}$$
$$\frac{dV_{C1}}{dt}=-\frac{1}{C_1}i_{L2};\ \frac{dV_{C2}}{dt}=-\frac{1}{C_2}i_{L2};\ \frac{dV_{C3}}{dt}=\frac{1}{C_3}\left(i_{L2}-i_o\right) \tag{1}$$

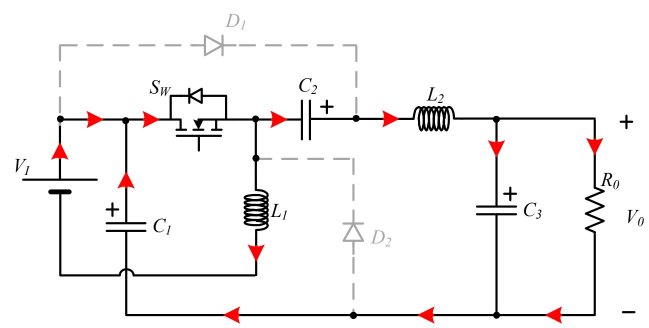

Fig. 2. Topological mode for the proposed converter when the transistor S_W is turned-on between 0 to δT_S

Switch S_W in OFF state: Based on the equivalent circuit presented in Fig. 3, in the *OFF*-state mode the transistor S_W is *OFF* during the time interval from δT_S to T_S. During this *OFF*-state diodes D_1 and D_2 are conducting. The stored energy of the inductor L_1 is discharged to the capacitor C_2 while the inductor L_2 discharges the energy stored to the output load. The state variable dynamics are given by (2).

$$\frac{di_{L1}}{dt}=\frac{V_I-V_{C2}}{L_1};\quad \frac{di_{L2}}{dt}=\frac{-V_0+V_{C2}}{L_2};$$
$$\frac{dV_{C1}}{dt}=\frac{1}{C_1}\left(\frac{i_{L1}-i_{L2}}{2}\right);\quad \frac{dV_{C2}}{dt}=\frac{1}{C_2}\left(\frac{i_{L1}-i_{L2}}{2}\right); \tag{2}$$
$$\frac{dV_{C3}}{dt}=\frac{1}{C_3}\left(i_{L2}-i_0\right);$$

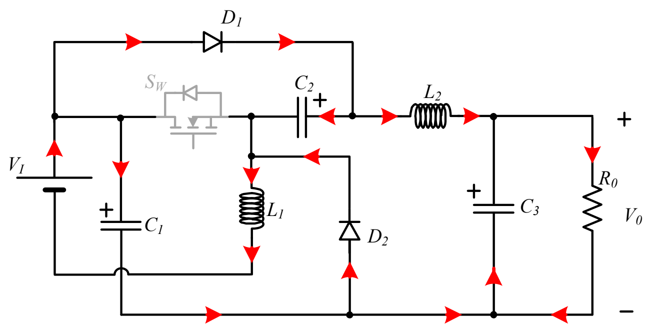

Fig. 3. Topological mode for the proposed converter when the transistor S_W is turned-off between δT_S to T_S

III. Analysis and Design of the Converter

A. Input to Output Voltage Gain

To determine the steady-state voltage gain of the proposed DC-DC converter, the analysis was conducted assuming CCM operation and ideal components. In steady-state operation, the average voltages across the inductors L_1 and L_2, designed as V_{L1} and V_{L2} respectively, must be equal to zero over a switching period.

$$V_{L1}=\delta V_I+\left(1-\delta\right)\left(V_I-V_{C1}\right)=0 \tag{3}$$

$$V_{L2}=\delta\left(V_{C1}+V_{C2}-V_o\right)+\left(1-\delta\right)\left(V_{C2}-V_o\right)=0 \tag{4}$$

Solving the previous equations, considering the voltages capacitors, C_1 and C_2 equals (V_{C1}=V_{C2}), the input to output voltage gain for the proposed converter, operation in CCM, is given by (5).

$$\frac{V_o}{V_I}=\frac{1+\delta}{1-\delta} \tag{5}$$

From the analysis of the previous expression, it is possible to see that this static gain is higher than the conventional Boost converter. The same conclusion can also be drawn from Fig. 4, which shows the static voltage gain V_O/V_I as a function of the duty cycle δ. The graph in Fig. 4 shows that the gain of the proposed converter increases more quickly than that of the conventional Boost converter when the δ increases, guaranteeing an extended static voltage gain in the input-output ratio.

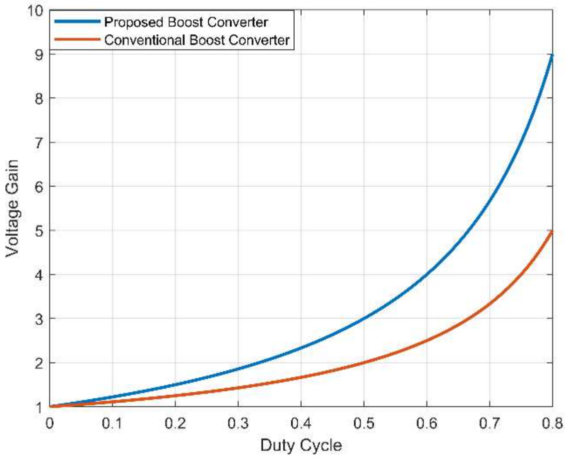

Fig. 4. Voltage gain for the conventional and the extended converter

B. Converter Design

The inductances and capacitances of the power converter have been designed with consideration for the maximum current and voltage ripple values in the inductors and capacitors, respectively, defined as Δ_L and Δ_{VC}. Consequently, this maximum value will be determined as a percentage of the inductor currents and a percentage of the capacitor voltage. Assuming quasi-linear variations for inductor currents and capacitor voltages, within the previous assumptions, it is possible to establish expressions for these components. Therefore, the inductor currents ripple, Δi_{L1} and Δi_{L2}, can be obtained from the respective inductor voltages, during the switch *ON* and switch *OFF* times, in the period $1/f_S$ (where f_S is the switching frequency). This way, considering the state switch *ON*, and V_I the voltage applied to the inductor, the L_1 inductance is a function of the current ripple ΔI_{L1}, as shown in the expression (5).

$$L_1 = \frac{\delta V_I}{\Delta I_{L1} f_S} \quad (5)$$

Based on the same reasoning, the inductance L_2 can be calculated when the state switch is *OFF* and V_{C2} as the voltage across the inductor, the L_2 is function of the current ripple ΔI_{L2}, defined by:

$$L_2 = \frac{V_{C2}(1-\delta)}{\Delta I_{L2} f_S} \quad (6)$$

A similar procedure was used to determine the size of the capacitors. In this case, considering relatively small voltage ripples, ΔV_{C1}, ΔV_{C2} and ΔV_{C3} regarding the average voltage of the capacitors, C_1, C_2, C_3, respectively. Based on the equations for capacitor currents, i_{C1}, i_{C2} and i_{C3}, during the switch *ON* time δT_S, the capacitance values are determined according to expressions (7).

$$C_1 = \frac{\delta I_{L2}}{\Delta V_{C1} f_S};\ C_2 = \frac{\delta I_{L2}}{\Delta V_{C2} f_S};\ C_3 = \frac{\delta(I_{L2} - I_o)}{\Delta V_{C3} f_S} \quad (7)$$

The precise design of the passive components in power electronic converters is crucial as they influence specifications such as size and weight. Analyzing the design of passive components reveals that the size of capacitors and inductors is inversely proportional to the switching frequency of the power semiconductors and to the allowed ripples.

Another aspect to consider in power converters is the maximum rating of the power semiconductors. These values are determined usually by the power supply or output voltages and by the output power of the converter. The voltage stress (V_{SW}) at the power switch (S_W) is obtained from circuit analysis in steady state, and given by equation (8), showing V_{SW} is smaller than the output voltage.

$$V_{SW\,\max} = V_{C2} = \frac{1}{1+\delta} V_o \quad (8)$$

The maximum average current of the power switch depends on the operating point of the power converter and the load current. Therefore, the current stress is given by (9).

$$I_{SW\,av\max} = \frac{2\delta}{1-\delta} I_0 \quad (9)$$

These expressions enable the selection of relatively low-voltage, high-current MOSFET transistors for the intended applications.

IV. Simulation Results

The time behavior of the proposed DC-DC converter was obtained based on numerical simulations, performed using Matlab/Simulink software and their Power Systems Toolbox. To validate the theoretical assumptions, presented previously, this DC-DC converter was evaluated in steady-state conditions first, and then under transient conditions. The following converter parameters were used for simulation tests: inductors L_1 = 10 mH and L_2 = 10 mH, capacitors C_1 = C_2 = 20 µF and C_3 = 100 µF. The switching frequency assumed was 10 kHz.

Steady-state simulation results were obtained with the proposed converter operating in a steady state, with a duty cycle of 0.6 and 100Ω load resistor. The waveforms presented in Fig. 5 show the input and output voltages, V_I and V_o, respectively, when the input voltage was equal to 50 volts. These results validate the static voltage theoretical gain obtained for the converter, as well as its extended conversion ratio when compared with the classical Boost in which for this duty cycle is obtained a lower static voltage gain. Compared to the conventional boost converter, it is seen a higher static voltage gain. Fig. 6 depicts the simulation waveforms of the L_1 and L_2 inductor currents. From these results it is possible confirm the CCM operation, with relatively small current ripples, in both inductors, compared to the current average values. The results of Fig. 6 also show that the current in inductor L_1 is on average 3.5 times greater than the current in inductor L_2. Fig.7 shows the voltages across the power semiconductor, S_W.

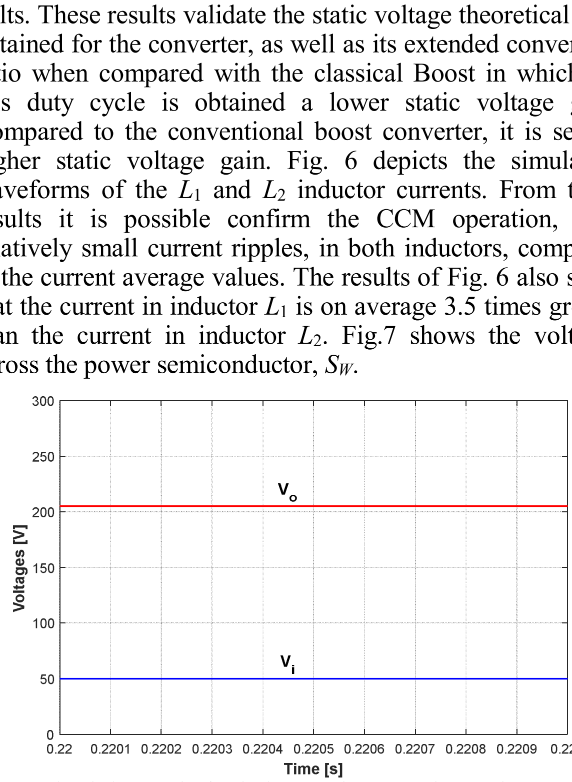

Fig. 5. Simulation results for the input and output voltage values

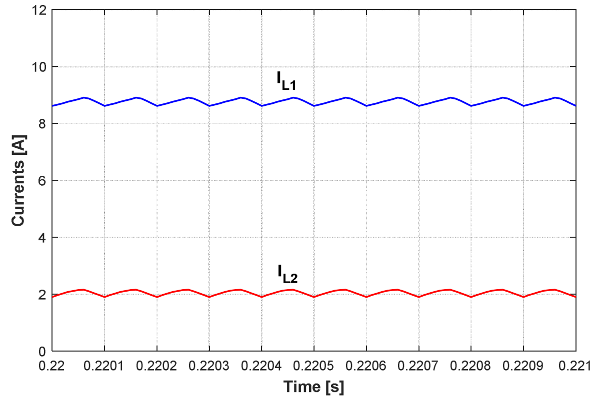

Fig. 6. Simulation results for the currents in both inductors L_1 and L_2

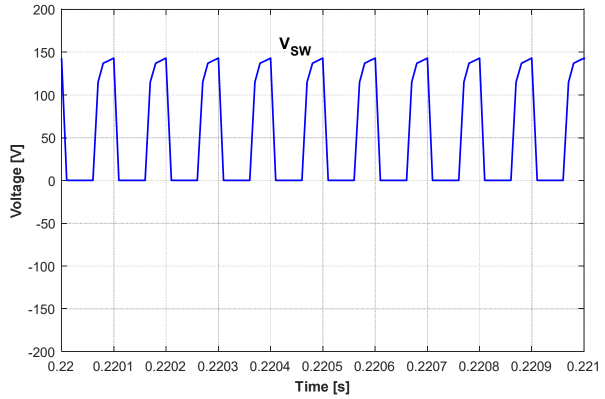

Fig. 7. Simulation results for the voltage across the power switch S_W

Based on the waveform analysis the *OFF*-state voltage on the transistor V_{SW}, is approximately 140 V, which is lower than the output voltage. This signifies that the power switch operates under reduced voltage stress, which is advantageous compared to topologies that require semiconductors capable of resisting the sum of input and output voltages.

The behavior of the converter was also simulated in order to assess the converter dynamic behavior. The results in Fig. 8 present the input and output voltages obtained by considering a sudden change in the duty cycle, δ, from 0.5 to 0.6 at t = 0.2s. Fig. 9 shows the waveforms of the L_1 and L_2 inductor currents, considering the previous dynamic conditions.

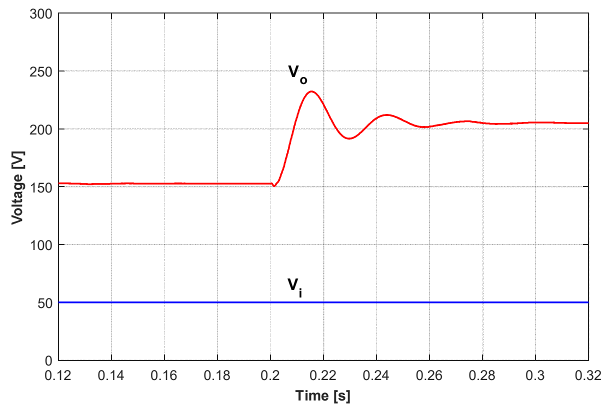

Fig. 8. Simulation results of the input and output voltage in transient mode, when there is a sudden change in the duty cycle, δ, from 0.5 to 0.6 at t = 0.2s

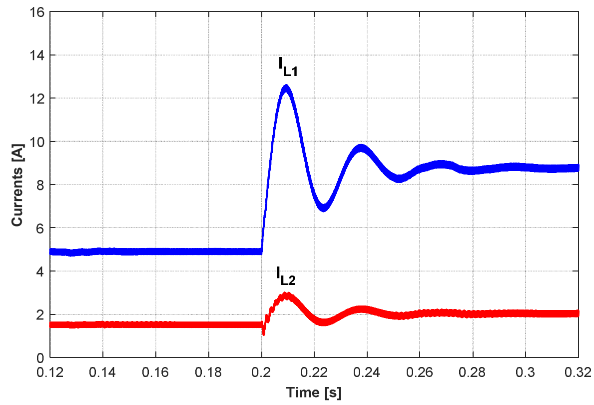

Fig. 9. Simulation results of the currents in both inductors L_1 and L_2 in transient mode, when there is a sudden change in the duty cycle, δ, from 0.5 to 0.6 at t = 0.2s

Analyzing these results it is concluded that when there is a step variation in the duty-cycle, the output voltage suffers a second order like disturbance. After the initial overshoot, a new steady-state value is reached. Based on these results, it can be said that the DC-DC output voltage and inductor currents present nearly a second order dynamics.

V. Experimental Results

To confirm the theoretical developments and the previous simulation results obtained from the proposed converter, an experimental prototype was built. The DC-DC converter was designed using parameters identical to those utilized in the numerical simulations. The carried-out laboratory tests used the same experimental procedures as the ones applied in the numerical simulations.

Figures 10 to 12 show the experimental results for the converter in a steady state, with a fixed duty cycle of 0.6 and a switching frequency f_S of 10 kHz. In Fig 10, the relationship between the absolute value of the output and input voltages is shown. This result shows that the voltage static gain is similar to that obtained by the simulation results, and at the same time confirming the theoretical analysis in (5). This experimental result also shows that the output voltage presents a smooth waveform with a very small ripple.

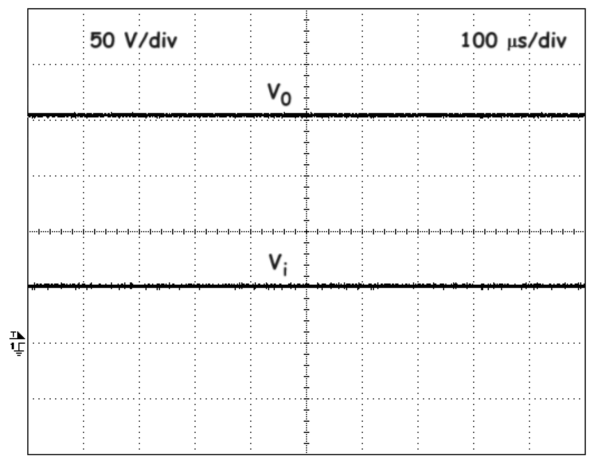

Fig. 10. Experimental results of the input and output voltages

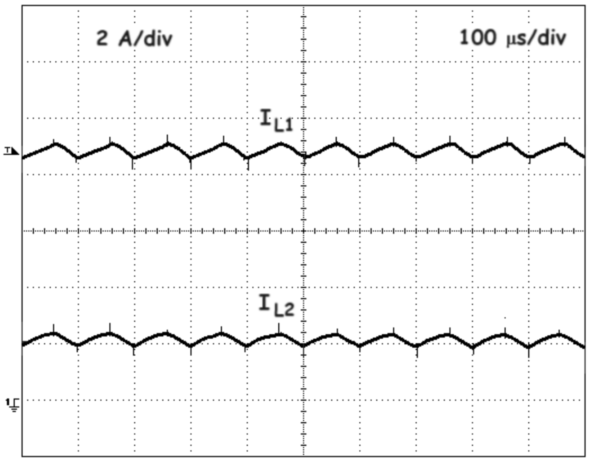

Fig. 11. Experimental results of the currents in both inductors L_1 and L_2

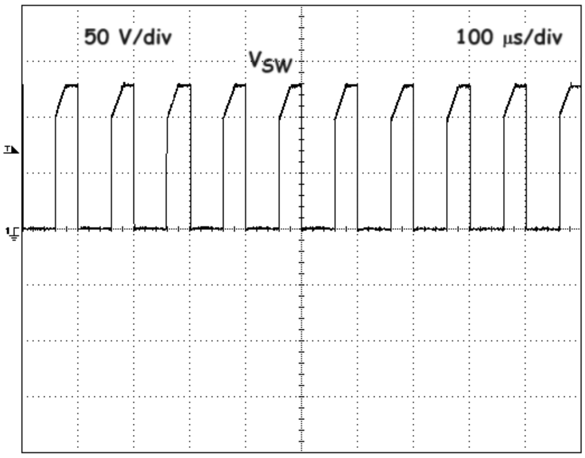

Fig. 12. Experimental results of the voltage across the power switch S_W

The waveforms for the inductor currents, I_{L1} and I_{L2}, are show in Fig. 11. These experimental results show continuous conduction mode in both inductors and a smaller current ripple in both waveforms, confirming the equivalent simulation result presented in Fig. 6. The experimental waveforms of the voltage on the power device (S_W) can be seen in Fig. 12. In this result it is seen that this device operates in state *OFF* holding-off voltages lower than the output voltage, confirming the expected characteristics of the converter.

As done in simulation tests, in the laboratory experiments the next results were obtained under dynamic conditions. The experimental results in Fig. 13 present the input and output voltages obtained by considering a step change in the duty cycle, δ, from 0.5 to 0.6 at t = 0.2s. Fig. 14 shows the waveforms of the L_1 and L_2 inductor currents, taking into account the previous dynamic conditions. Through the analysis of these results, it is possible to verify that when there is a step variation in the duty-cycle, the output voltage presents a second order like behavior, together with the inductor currents. These experimental results confirm the converter maintains the CCM even in these transient conditions.

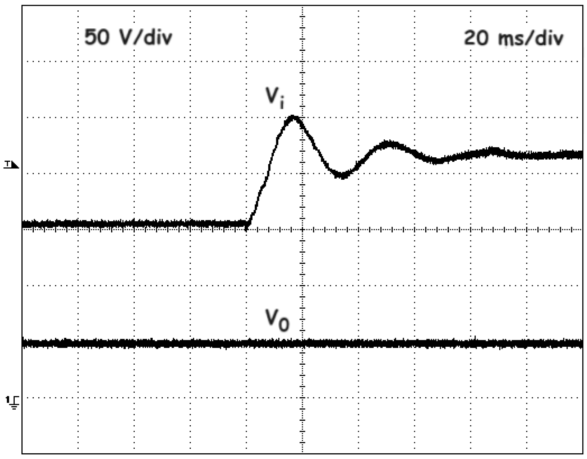

Fig. 13. Experimental results of the input and output voltage in transient mode, when there is a sudden change in the δ from 0.5 to 0.6 at t = 0.2s

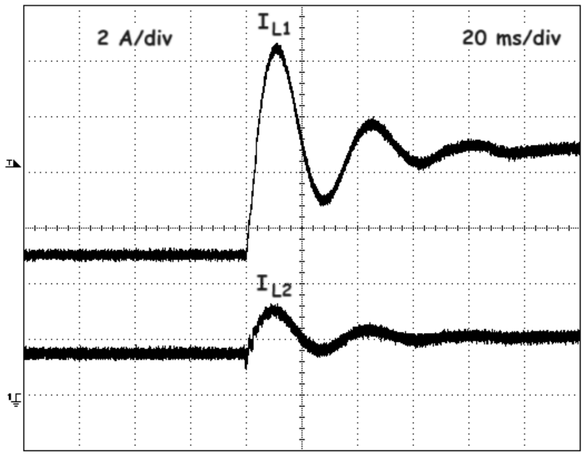

Fig. 14. Experimental results of the currents in both inductors L_1 and L_2 in transient mode, when there is a sudden change in the duty cycle, δ, from 0.5 to 0.6 at t = 0.2s

VI. CONCLUSIONS

In this work, a new topology for DC-DC Boost converters with an extend voltage static gain is proposed. Step-up converters are very important in many applications, particularly those requiring high static voltage gains. This is particularly relevant for renewable energy applications, where solar power may be affected by shading effects, as well as for applications using fuel cell systems. The proposed DC-DC converter topology uses a single controlled power switch and its topology offers an extended voltage gain characteristic, achieving higher voltage gains with reduced duty ratios compared to standard boost topologies. Additionally, this converter provides continuous input and output currents with low ripple and reduced voltage stress on the power switch and diodes. An analysis of the converter's operating states and the formulation of the static voltage gain were presented. The static voltage gain and the nearly second order dynamic behavior of the proposed converter was evaluated through computer simulations and practical experiments using a laboratory prototype. The results allowed to confirm the reduced voltage stress on the power semiconductor and reduced ripple in the input current.

ACKNOWLEDGMENT

This work was supported by national funds through FCT, Fundação para a Ciência e a Tecnologia, under project UIDB/50021/2020 (DOI:10.54499/UIDB/50021/2020).

REFERENCES

[1] Kjaer, S.B.; Pedersen, J.K.; Blaabjerg, F. Power inverter topologies for photovoltaic modules-a review. In Proceedings of the Conference Record of the 2002 IEEE Industry Applications Conference. 37th IAS Annual Meeting (Cat. No. 02CH37344), Pittsburgh, PA, USA, 13–18 October 2002; Volume 2, pp. 782–788.

[2] Hossain, M.Z.; Rahim, N.A.; Selvaraj, J. Recent progress and development on power DC-DC converter topology, control, design and applications: A review. *Renew. Sustain. Energy Rev.* 2018, *81 Pt 1*, 205–230.

[3] Murillo-Yarce, D.; Restrepo, C.; Lamar, D.G.; Hernando, M.M.; Sebastián, J. Study of Multiple Discontinuous Conduction Modes in SEPIC, Ćuk, and Zeta Converters. *Electronics* 2022, *11*, 3744.

[4] V. F. Pires, A. Cordeiro, C. Roncero-Clemente, S. Rivera and T. Dragičević, "DC–DC Converters for Bipolar Microgrid Voltage Balancing: A Comprehensive Review of Architectures and Topologies," in IEEE Journal of Emerging and Selected Topics in Power Electronics, vol. 11, no. 1, pp. 981-998, Feb. 2023.

[5] I. Lee, "Hybrid DC–DC Converter With Phase-Shift or Frequency Modulation for NEV Battery Charger," IEEE Transactions on Industrial Electronics, 2016, vol. 63, no. 2, pp. 884-893.

[6] Hattori, S.; Eto, H.; Kurokawa, F. High Power Density Battery Charger for Plug-In Micro EV. *Int. J. Renew. Energy Res.* **2018**, *8*, 1006–1015.

[7] V. F. Pires, D. Foito and A. Cordeiro, "A DC–DC Converter With Quadratic Gain and Bidirectional Capability for Batteries/Supercapacitors," in IEEE Transactions on Industry Applications, vol. 54, no. 1, pp. 274-285, Jan.-Feb. 2018.

[8] Paragond, L.; Kurian, C.; Singh, B.; Jyothi, A. Simulation and Control of DC/DC Converter for MPPT Based Hybrid PV/Wind Power System. *Int. J. Renew. Energy Res.* **2014**, *4*, 801–809.

[9] Raghavendra, K.V.G.; Zeb, K.; Muthusamy, A.; Krishna, T.N.V.; Kumar, S.V.S.V.P.; Kim, D.-H.; Kim, M.-S.; Cho, H.-G.; Kim, H.-J. A Comprehensive Review of DC–DC Converter Topologies and Modulation Strategies with Recent Advances in Solar Photovoltaic Systems. *Electronics* **2020**, *9*, 31.

[10] Ellabban, O.; Abu-Rub, H.; Blaabjerg, F. Renewable energy resources: Current status, future prospects and their enabling technology. *Renew. Sustain. Energy Rev.* 2014, *39*, 748–764.

[11] P. K. Maroti, S. Padmanaban, F. Blaabjerg, P. Wheeler and L. Martirano, "A Novel High Gain Non-Inverting, Single Switch Configurations of Modified SEPIC DC-DC Converter for High-Voltage/Low-Current Renewable Energy Applications," European Conference on Power Electronics and Applications (EPE'18 ECCE Europe), 2018, pp. 1 9.

[12] A. Chub, D. Vinnikov, F. Blaabjerg and F. Z. Peng, "A Review of Galvanically Isolated Impedance-Source DC–DC Converters," IEEE Transactions on Power Electronics, 2016, vol. 31, no. 4, pp. 2808-2828.

[13] S. A. Gorji, H. G. Sahebi, M. Ektesabi and A. B. Rad, "Topologies and Control Schemes of Bidirectional DC–DC Power Converters: An Overview," IEEE Access, 2019, vol.7, pp. 117997-118019.

[14] Liu H., Hu H., and Wu H. et al.: 'Overview of high step-up coupled-inductor boost converter', IEEE J. Emergy Select. Top. Power Electron., 2016, 4, (2), pp. 689–704.

[15] A. A. Khan, M. Jamil, U. A. Khan, I. Khan, W. Eberle and S. Ahmed, "Novel Three and Four Switch Inverters With Wide Input and Output Voltage Range for Renewable Energy Systems," in IEEE Journal of Emerging and Selected Topics in Power Electronics, vol. 10, no. 6, pp. 7385-7396, December 2022.

[16] J. Monteiro, V. F. Pires, D. Foito, A. Cordeiro, J. F. Silva, S. A. Pinto, "A Buck-Boost Converter with Extended Duty-Cycle Range in the Buck Voltage Region for Renewable Energy Sources.", Electronics, vol. 12, no. 3, pp. 1-20, February 2023.

[17] C. Rani, CH Hussain Basha, Sarah odofin, " A Review on Non-isolated Inductor Coupled DC-DC Converter for Photovoltaic Grid-Connected Applications," International Journal of Renewable Energy Research, vol.7, no. 4, pp. 1570-1585, December 2017.

[18] V. F. Pires, D. Foito, F.R.B. Baptista, J. F. Silva, "A photovoltaic generator system with a DC/DC converter based on an integrated Boost-Ćuk topology," Solar Energy, vol. 136, pp. 1-9, October 2016.

[19] S. Belhimer, M. Haddadi, A. Mellit, "A novel hybrid boost converter with extended duty cycles range for tracking the maximum power point in photovoltaic system applications",International Journal of Hydrogen Energy, Volume 43, Issue 14, 2018. Pages 6887-6898

[20] S. H. Hosseini, R. S. Alishah and K. V. Kurdkandi, "Design of a new extended zeta converter with high voltage gain for photovoltaic applications," 9th International Conference on Power Electronics and ECCE Asia (ICPE-ECCE Asia), 2015, pp. 970-977.

[21] M. Banaei and S. Sani, "Analysis and Implementation of a New SEPIC-Based Single-Switch Buck–Boost DC–DC Converter With Continuous Input Current," IEEE Transactions on Power Electronics, 2018, vol. 33, no. 12, pp. 10317-10325.

[22] K. Çelik, M. Demirtas and N. Öztürk, "Analytical Investigation of PV Panel Operated at Maximum Power Point on DC Microgrid," 11th International Conference on Renewable Energy Research and Application (ICRERA), pp. 324-329, September 2022.

[23] Chen, J.; Maksimovic, D.; Erickson, R.W. "Analysis and design of a low-stress buck boost converter in universal-input PFC applications". IEEE Trans. Power Electron. 2006

[24] S. M. Fardahar and M. Sabahi., "New Expandable Switched-Capacitor/Switched-Inductor High-Voltage Conversion Ratio Bidirectional DC–DC Converter," IEEE Transactions on Power Electronics, 2020, vol. 35, no. 3, pp. 2480-2487.

[25] V. F. Pires, A. Cordeiro, D. Foito and J. F. Silva, "High Step-Up DC–DC Converter for Fuel Cell Vehicles Based on Merged Quadratic Boost–Ćuk," in IEEE Transactions on Vehicular Technology, vol. 68, no. 8, pp. 7521-7530, Aug. 2019.

[26] N. Zhang, G. Zhang, K. See and B. Zhang, "A Single-Switch Quadratic Buck–Boost Converter With Continuous Input Port Current and Continuous Output Port Current," IEEE Transactions on Power Electronics, 2018, vol. 33, no. 5, pp. 4157-4166.